[3] Hanna, G. L., Troiano, A. R., and Steigerwald, E. A., "A Mechanism for Embrittlement of High Strength Steels by Aqueous Environments," *Transactions American Society for Metals*, Vol. 57, 1964, pp. 658–671.

[4] Dull, D. L. and Raymond, L., "A Method of Evaluating Relative Susceptibility of Bolting Materials to Stress Corrosion Cracking," presented at 1972 Westec Conference, March 1972; also *Corrosion*, to be published.

[5] Phillips, A., Kerlins, V., and Whiteson, B. V., "Electron Fractographic Handbook," AFML Rept. ML-TDR-64-416, Aug. 1968, Air Force Materials Lab., Wright-Patterson Air Force Base, Ohio.

[6] Fidelle, J. P., Legrand, J., and Couderc, C., "A Fractographic Study of Hydrogen Gas Embrittlement in Steels," *Transactions of the American Institute of Mining, Metallurgical Engineers*, 1972, to be published.

[7] Tiner, N. A. and Filpin, C. B., "Microprocesses in Stress Corrosion of Martensitic Steels, *Corrosion*, Vol. 22, 1966, pp. 271–279.

[8] Brown, B. F., "A New Stress Corrosion Cracking Test for High Strength Alloys," *Materials Research and Standards*, Vol. 16, March 1966, pp. 129–133.

[9] Brown, B. F., "The Application of Fracture Mechanics to Stress-Corrosion Cracking," *Metallurgical Review*, Vol. 13, 1968, pp. 171–183.

[10] Mulherin, J. H., "Stress Corrosion Susceptibility of High Strength Steel in Relation to Fracture Toughness," *Transactions of the ASME: Journal of Basic Engineering*, Vol. 88, 1966, pp. 772–782.

[11] Tentative Method of Test for Plane-Strain Fracture Toughness of Metallic Materials, E399-70T, *Book of Standards*, American Society for Testing and Materials, Philadelphia, Pt. 31, July 1971, pp. 911–1927.

[12] Freedman, A. J., "Development of an Accelerated Stress-Corrosion Test for Ferrous and Nickel Alloys," Finary Summary Rept., NOR 68-58, April 1968, Northrop Corp., Hawthorne, Calif.

NOVEMBER 1972 J. SPACECRAFT VOL. 9, NO. 11

Application of an Improved Transpiration Cooling Concept to Space Shuttle Type Vehicles

JOHN R. SCHUSTER* AND THOMAS G. LEE†
McDonnell Douglas Astronautics Company—West
Huntington Beach, Calif.

In order to reduce coolant requirements transpiration cooled structures should be operated at the maximum possible surface temperature. At high-surface temperature a flow instability can occur, because of the pressure drop characteristics of gases, leading to burnout of the porous structure. This instability can be avoided by overlaying the sintered metallic structure with a ceramic coating of much higher permeability. By applying this design concept to the leading-edge and interference heating regions of a space shuttle type vehicle substantial reductions can be realized in coolant requirement. Since the thickness of the ceramic layer is inversely proportional to the required coolant flow rate, the leading-edge coolant savings are offset by increasing structure weight. For interference heating, however, the ceramic layer is thin and large net savings in weight can be obtained.

Nomenclature

C_p = specific heat, Btu/lbm-°R
D = diameter, ft
g_c = conversion factor, 32.17 lbm-ft/lbf-sec^2
H = enthalpy, Btu/lbm
ΔH = net enthalpy rise in coolant, Btu/lbm
k = conductivity, Btu/ft-sec-°R
L = length, ft
M = coolant molar weight, lbm/lb-mole
$\dot{m}$ = coolant flux, lbm/ft^2-sec
N_C = convective heat-transfer coefficient, lbm/ft^2-sec
P = pressure, lbf/ft^2
Q_c = convective heat flux, Btu/ft^2-sec
R = gas constant, lbf-ft/lb-mole-°R
T = temperature, deg R
α = porous matrix viscous pressure drop constant, ft^{-2}
β = porous matrix inertial pressure drop constant, ft^{-1}
ε = effective emissivity of surface, dimensionless
γ = porous matrix void fraction, dimensionless
Γ = porous matrix tortuosity for heat conduction, dimensionless
μ = coolant viscosity, lbm/ft-sec
ρ = coolant density, lbm/ft^3
σ = Stefan-Boltzmann constant, 0.476×10^{-12} Btu/ft^2-sec-°R^4
$\bar{\sigma}$ = elemental surface area normal vector, ft^2
θ = included angle between $\bar{\sigma}$ and freestream vector, rad

Subscripts

A = value at point A
B = value at point B
C = value for coolant
e = effective value
l = value for coolant liquid phase
o = value without transpiration cooling or value in coolant storage reservoir
pore = value for pore within the porous matrix
r = recovery value
s = value for freestream species evaluated at surface temperature and pressure

Submitted April 17, 1972; revision received July 17, 1972. This work was supported by McDonnell Douglas Independent Research and Development funds, and was performed under the direction of James E. Rogan.

Index categories: Heat Conduction; Boundary Layers and Convective Heat Transfer—Laminar; Structural Composite Materials (Including Coatings).

* Senior Engineer Scientist, Aerothermodynamics.
† Section Chief. Heat Transfer and Materials Performance.

sink = sink for thermal radiation
stag = value at stagnation line
struct = value for structure parent material
v = value for coolant vapor phase

Introduction

TRANSPIRATION cooling thermal protection systems have long been considered for use in regions where high heating rates exist. This type of a system is particularly applicable in these regions since it is the only thermal protection method which does not have an upper heating rate limitation. Some current uses of transpiration cooling are rocket nozzles, re-entry vehicle nose tips and turbine vanes.

Considerable experimental and analytic work has recently been conducted[1-5] to identify regions of high heating on space shuttle type vehicles. Although the results are very configuration oriented, it is clear that reuseable high-heating thermal protection will be required over at least limited areas. Recognizing the need for an acceptable design approach, parametric studies of both passive and active thermal protection concepts were conducted for leading edges[6, 7] and it was concluded that no single system meets all performance objectives, i.e., passive systems are reuse limited due to surface recession, and active systems limit mission flexibility due to excessive weight penalty. Of the active systems considered, liquid film transpiration cooling with water was judged the most efficient.

Transpiration cooling efficiency can be increased by operating at high-surface temperature. For a liquid coolant this implies phase change within the porous material. Whether the coolant is initially a liquid or gas, operational instability can result at high temperature due to the relationship between coolant viscosity and temperature. This instability problem can be avoided if a dual layer material is used with the following properties. The inner layer must have a low permeability in order to control coolant flow and the outer layer must have a low-thermal conductivity and a high permeability so as to buffer the inner layer from high temperature and yet not develop a high back pressure.

The present paper therefore is devoted to evaluating specific design aspects of transpiration cooling as applied to high heating areas on space shuttle type vehicles. In addition, a dual layer, high-temperature transpiration cooling design approach is described that will permit significant weight reductions when used in areas subjected to severe interference heating. For reasons of expediency, the space shuttle delta wing orbiter leading edge has been chosen as a baseline for the analysis.

Analysis

The basic approach generally used to analyze transpiration cooling is to decouple the porous matrix flow and boundary-layer flow. This is done by assuming surface temperature distributions and boundary layer similarity such that thermally ideal coolant flux distributions can be evaluated for the heated surface. The porous structure is then designed such that its hydraulic characteristics result in an actual coolant distribution that closely matches the thermally ideal distribution.

Mass Transfer

From a surface energy balance the following equation can be written

$$Q_{c_o} = \frac{\varepsilon\sigma(T_s^4 - T_{\text{sink}}^4) + \dot{m}\Delta H}{N_c/N_{c_o}} \tag{1}$$

where Q_{c_o} is the surface convective heat flux without mass transfer, ΔH is the net enthalpy rise of the coolant, including subcooling, heat of vaporization, and surface superheat, and N_c/N_{c_o} represents the apparent reduction in heat-transfer coefficient due to the mass transfer blocking occurring in the boundary layer. The no-blowing surface convective heat flux can also be expressed as

$$Q_{c_o} = N_{c_o}(H_r - H_s) \tag{2}$$

where $(H_r - H_s)$ is the difference between the recovery enthalpy and the enthalpy evaluated at the local surface pressure and assumed surface temperature.

Bartle and Leadon,[8] Rubesin,[9] and Arne[10] have presented design correlations, based on similarity, for the ratio N_c/N_{c_o}. The correlations of Arne are presented here. For a laminar boundary layer,

$$\frac{N_c}{N_{c_o}} = 1.0 - \left(\frac{C_{pv}}{C_{ps}}\right)^{0.4}\left[0.68\,\frac{\dot{m}}{N_{c_o}} - 0.08\left(\frac{\dot{m}}{N_{c_o}}\right)^2\right] \tag{3}$$

For a turbulent boundary layer,

$$\frac{N_c}{N_{c_o}} = \frac{(C_{pv}/C_{ps})^{0.8}\dot{m}/N_{c_o}}{[1.0 + 0.25(C_{pv}/C_{ps})^{0.8}\dot{m}/N_{c_o}]^4 - 1.0} \tag{4}$$

where C_{pv}/C_{ps} is the ratio between the coolant vapor specific heat and freestream species specific heat, evaluated at the local surface pressure and specified local surface temperature.

For the laminar case Eqs. (1-3) are solved explicitly for the thermally ideal coolant flux.

$$\dot{m} = 6.25N_{c_o}\left(\frac{C_{pv}}{C_{ps}}\right)^{-0.4}(H_r - H_s)^{-1.0} \times \left\{0.68\left(\frac{C_{pv}}{C_{ps}}\right)^{0.4}(H_r - H_s) + \Delta H - \left(\left[0.68\left(\frac{C_{pv}}{C_{ps}}\right)^{0.4}(H_r - H_s) + \Delta H\right]^2 - 0.32\left(\frac{C_{pv}}{C_{ps}}\right)^{0.4}(H_r - H_s) \times \left[H_r - H_s - \frac{\varepsilon\sigma}{N_{c_o}}(T_s^4 - T_{\text{sink}}^4)\right]\right)^{0.5}\right\} \tag{5}$$

For the turbulent case a technique such as Newton-Raphson linear iteration must be used on the coolant flux, utilizing Eq. (4), until the heat flux calculated with Eq. (1) is equal to that of Eq. (2).

Based on the previous equations, Fig. 1 presents thermally ideal coolant fluxes for water as a function of boundary layer enthalpy potential, surface temperature, and no-blowing surface heat-transfer coefficient. It can be seen by examining Eqs. (1-5) that for high heat-transfer coefficients, a solution is approached in the form of the dimensionless ratio $\dot{m}/N_{c_o}$. It can be seen from Fig. 1 that for the range of surface temperature presented, the ratio becomes essentially independent of N_{c_o} at a value of 1.0.

Porous Matrix

The steady-state porous matrix coolant flow solution is based on the following equations: continuity,

$$\oint_s (\bar{\dot{m}}) \cdot d\bar{\sigma} = 0 \tag{6}$$

the modified Darcy equation for pressure drop,

$$-g_c\nabla P = \left(\alpha\,\frac{\mu}{\rho} + \beta\,\frac{\dot{m}}{\rho}\right)\bar{\dot{m}} \tag{7}$$

and the porous flow energy equation,

$$-k_e\nabla^2 T - (\nabla k_e)\cdot(\nabla T) + \nabla\cdot(H\bar{\dot{m}}) = 0 \tag{8}$$

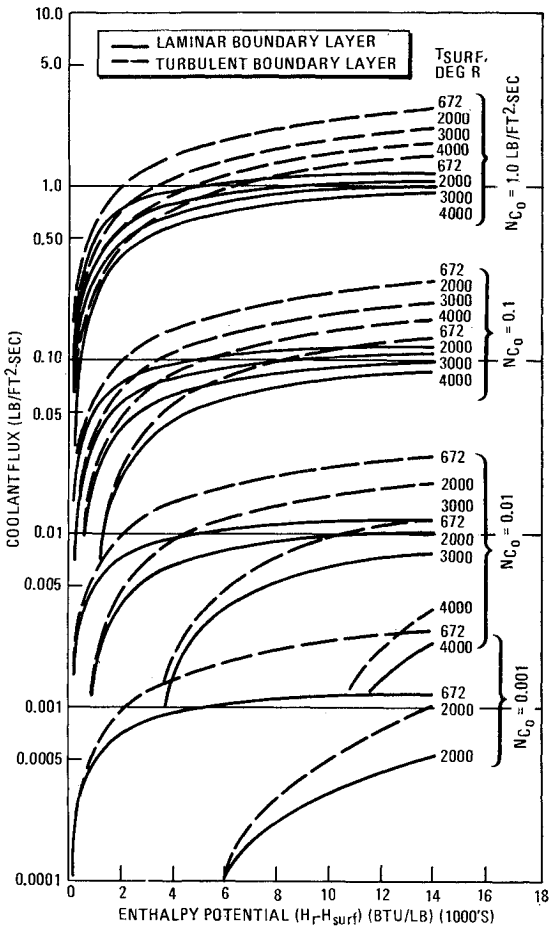

Fig. 1 Ideal coolant flux for water.

The viscous pressure drop constant α is the inverse of the porous matrix permeability, and the constant β is to account for additional pressure drop due to inertial effects. The inertial term becomes increasingly important for higher coolant fluxes, however for coolant fluxes that will be required on space shuttle type vehicles, this term can generally be ignored. If the coolant is in the vapor state within the porous matrix, the perfect gas law can be utilized in conjunction with Eq. (8) to eliminate coolant density from the pressure drop equation, yielding

$$-g_c\nabla P^2 = 2MRT(\alpha\mu - \beta\dot{m})\dot{m} \tag{9}$$

The local effective thermal conductivity is that of the coolant infiltrated matrix, and is determined by the following equation

$$k_e = \gamma k_c + (1.0 - \Gamma)(1.0 - \gamma)k_{\text{struct}} \tag{10}$$

where γ is the porous matrix void fraction and Γ is the porous matrix tortuosity. The tortuosity term, which varies between zero and one, is included to represent the heterogenous nature of the porous structure, and accounts for the effect of contact resistance and pore shape on structure thermal conductivity. Tortuosity must be evaluated experimentally.

Equation (8) assumes that the coolant within a pore and the surrounding pore material are in thermal equilibrium. Assuming that purely laminar flow exists within the porous material, a one-dimensional analysis based on a spherical pore geometry yields the following equation for the local temperature differential within the porous matrix.

$$T_{\text{pore}} - T_c = 0.0625 D_{\text{pore}}^2(\dot{m})^2 \frac{C_{pc}}{\gamma k_c k_e}(\Delta H) \tag{11}$$

For a relatively large pore diameter of 20 μ, and conditions representative of space shuttle type interference heating (a surface temperature of 4000°R and a coolant flux of 0.07 lb/ft²-sec) the temperature differential between the coolant and surrounding pore material is 0.2°R, and therefore can be ignored.

One-Dimensional Porous Flow Approximations

For space shuttle type vehicles, surface pressures and pressure gradients over the surface will be very low, making it possible to obtain good porous flow estimates from one-dimensional approximations to Eqs. (6–9). For liquid flowing from point A to point B within the matrix, the temperature at point A can be related to that at point B by the following variation of the energy equation

$$T_A = T_o + (T_B - T_o)\exp[-(\dot{m}C_{pl}/k_e)L_{A-B}] \tag{12}$$

where L_{A-B} is the distance separating the two points, and T_o is the coolant reservoir temperature. The pressure drop equation can be simplified to

$$P_A = P_B + (\alpha\dot{m}\mu_l/g_c\rho_l)L_{A-B} \tag{13}$$

where the effective liquid viscosity can be approximated by evaluating it at the following temperature

$$T = T_o + \frac{(T_B - T_o)k_e}{\dot{m}C_{pl}L_{A-B}}\left[1.0 - \exp\left(-\frac{\dot{m}C_{pl}}{k_e}L_{A-B}\right)\right] \tag{14}$$

For vapor flowing from point A to point B the energy equation becomes

$$T_A = T_B - \left(\frac{H_B - H_o}{C_{pv}}\right)\left[1.0 - \exp\left(-\frac{\dot{m}C_{pv}}{k_e}L_{A-B}\right)\right] \tag{15}$$

The pressure drop equation for the vapor can be simplified to

$$P_A^2 = P_B^2 + \frac{2\alpha R\mu_v}{Mg_c} \times \left\{\frac{H_B - H_o}{C_{pv}^2}k_e\left(1.0 - \exp\left[-\frac{\dot{m}C_{pv}}{k_e}L_{A-B}\right]\right) + \dot{m}L_{A-B}\left(T_B - \frac{H_B - H_o}{C_{pv}}\right)\right\} \tag{16}$$

where the effective vapor viscosity can be approximated by evaluating it at the following temperature

$$T = T_B - \frac{H_B - H_o}{C_{pv}} + \frac{H_B - H_o}{\dot{m}C_{pv}^2 L_{A-B}}k_e\left[1.0 - \exp\left(-\frac{\dot{m}C_{pv}}{k_e}L_{A-B}\right)\right] \tag{17}$$

High-Surface Temperature Transpiration Cooling

It can be seen from Fig. 1 that reductions in coolant requirement can be obtained by operating at elevated surface temperature. This becomes increasingly significant as heat-transfer coefficient decreases because larger fractions of the convective heat flux can be radiated back by the high-temperature surface, resulting in less heat being conducted into the structure.

Coolant Phase Change Instability

Figure 2 illustrates the pressure drop characteristics of both liquid and vapor water. It can be seen that as long as the coolant is in the liquid phase, flow resistance tends to decrease with increasing coolant temperature. When this phenomena

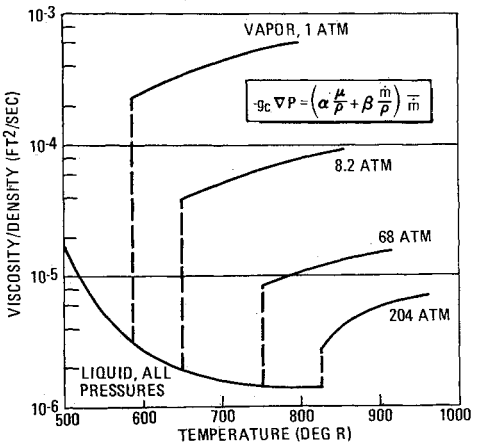

Fig. 2 Pressure drop parameter for water.

is coupled to a fixed external boundary-layer heating condition, any increase in coolant flow will cause a decrease in surface temperature and subsequently an increase in coolant flow resistance. This is a stable characteristic and results in the ability to set coolant flow rate by controlling coolant supply pressure. However, if the surface temperature is allowed to exceed the local coolant vaporization temperature such that coolant phase change takes place within the porous matrix, not only is there a large discontinuous increase in local flow resistance, but flow resistance tends to increase with increasing temperature. This is an unstable trend, and can result in the inability to control coolant flow by varying supply pressure, thus resulting in runaway surface temperature and possible porous structure burnout.

Dual Layer Concept

Upon some consideration it can be seen that positive control over coolant flow rate can be maintained if the major part of the pressure differential between the porous structure inner and outer surface occurs while the coolant is in the liquid phase. This will retain some measure of the pressure drop characteristic typical of liquid, as illustrated in Fig. 2. One approach to achieving positive flow control is to utilize a porous matrix consisting of two layers of material with widely different properties. Figure 3 illustrates the properties desired of these materials. The inner layer is a high-strength, low-porosity metal that regulates the coolant flow and provides structural strength. The outer layer is a high-temperature, high-porosity, low-thermal conductivity material that can buffer the inner layer against high temperature and also permit coolant phase change without creating a large back pressure.

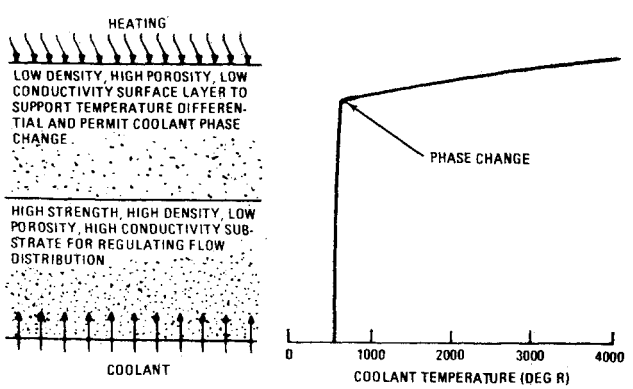

Fig. 3 High-surface temperature transpiration material properties.

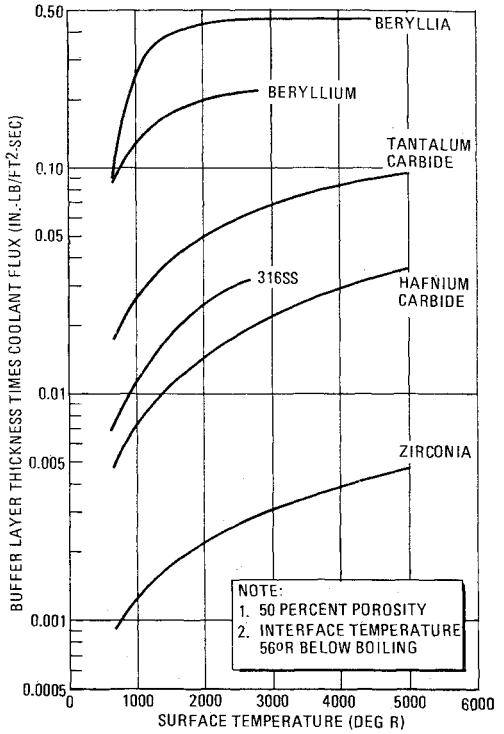

Fig. 4 Buffer layer thickness requirements.

From Eqs. (12) and (15) it can be seen that for a given type of material and a fixed surface temperature, buffer layer thickness requirement is inversely proportional to coolant flux. From a physical standpoint this is readily reasoned if one considers that the amount of buffer layer required to yield a specified interface temperature is inversely proportional to the temperature gradient established within the layer. As indicated by calculations performed using Eq. (11), the temperature of the coolant in a pore and of the surrounding pore material are essentially the same. Therefore the amount of heat absorbed by the coolant as it flows through the buffer layer is proportional to coolant flow rate, thus making the temperature gradient in the buffer layer proportional to flow rate.

Figure 4 illustrates, for a range of materials, buffer layer thickness requirements as determined from a finite difference one-dimensional analysis using Eq. (8). Since test data does not exist, and to be conservative, the material tortuosity has been assumed to be zero. So as to ensure that coolant phase change takes place within the buffer layer, the layer thickness calculations were based on obtaining 56° of coolant subcooling at the buffer layer/structure interface.

In general the ceramics make the best buffer layer because of their low thermal conductivity. Of the materials studied, zirconia appears most attractive, not only because it results

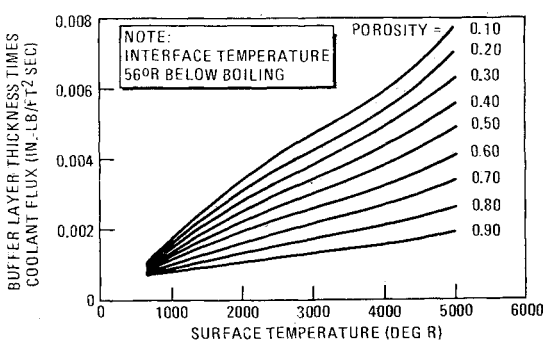

Fig. 5 Zirconia buffer layer thickness requirements.

in the thinnest buffer layers, but: a) its crystalline form can be stabilized by additives such as yttria; b) it has a coefficient of thermal expansion close to that of stainless steel; c) it is unreactive at high temperature to either air or water vapor; and d) it has a melting temperature of approximately 5200°R. In addition it is widely used in many forms as a thermal insulator, resulting in relatively low cost for the raw material.

Figure 5 presents detailed buffer layer thickness requirements for zirconia of various porosities and zero tortuosity. In order to reduce coolant vapor phase pressure drop it is desirable to have a high porosity. In this instance, pressure drop requirements are also consistent with thermal requirements, as increasing porosity also results in thinner zirconia layers being required to buffer the porous metallic substrate.

Porous Matrix Permeability Requirements

Porous matrix permeability must be linked to available coolant pressure in order that the proper flow of coolant be supplied to the heated surface. For the dual layer high-temperature concept, the relative permeability of the two materials must also result in the major portion of the coolant pressure drop being allocated to the inner metallic structure. This is so that stable operation can be achieved and coolant flow rate can be changed by regulating supply pressure. Although it is not clear what an acceptable minimum ratio between pressure drops is, a value of ten should provide for adequate flow control.

For a 0.050 in. thick, inner porous structure, Fig. 6 presents both zirconia buffer layer and structure permeability requirements as a function of available coolant supply pressure and buffer layer surface temperature. For the buffer layer, thermal considerations dictate a thickness that is inversely proportional to coolant flux, therefore for a given surface temperature, buffer layer pressure drop is essentially independent of coolant flux. For the buffered inner metallic structure, however, coolant temperature and viscosity change only slightly with flow rate therefore making structure permeability proportional to flow rate.

Application to Shuttle Type Leading Edge

Although the previously described analysis and transpiration cooling design approach can be applied to any region of high heating on a shuttle type vehicle, the remainder of this paper deals with the Orbiter wing leading edge, for which the heating environment can be relatively well defined. In addition to ordinary leading-edge heating, an interference region is postulated in order to illustrate the reduction in weight offered by the dual layer high-surface temperature concept.

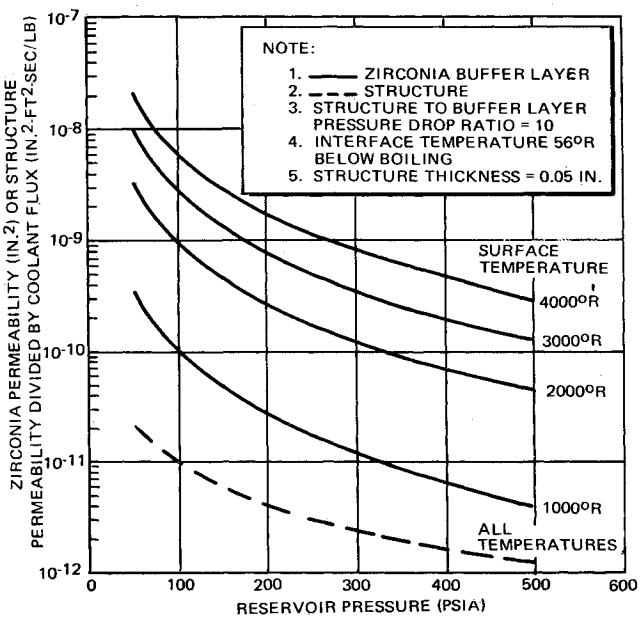

Fig. 6 Buffer layer and structure permeability requirements.

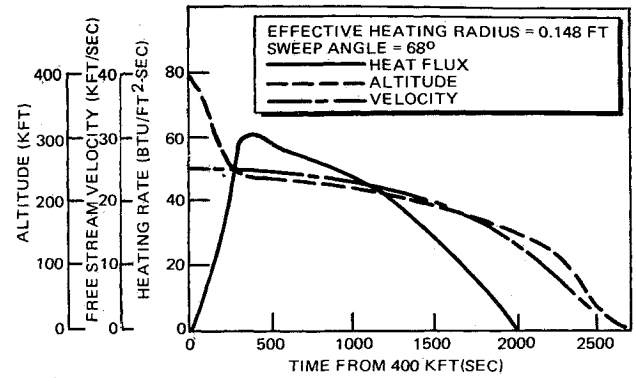

Fig. 7 Delta wing Orbiter trajectory and stagnation line heating.

Leading-Edge Heating

Figure 7 presents the assumed trajectory and resultant stagnation line laminar heating for the leading edge, as determined by Parks and Bauer.[6] It is for a delta wing Orbiter with a sweep angle of 68°, and an effective leading-edge heating radius of 0.148 ft. For the purpose of evaluating coolant requirements, a cylindrical leading edge will be assumed.

Heating in the interference region is assumed turbulent, and is obtained by applying the Mach number dependent multiplier shown in Fig. 8. Above a freestream Mach number of 10, a constant multiplier of 20 is used. Although the conditions upon which the data is based are not necessarily the same as for shuttle type vehicles, recent wind-tunnel data[1-4] for various shuttle configurations indicates, qualitatively, the same trends.

The coolant distributions assumed for the leading edge are proportional to the expected heating distribution, and are conservative in the respect that they ignore the amplified effect high-surface temperature would have on reducing

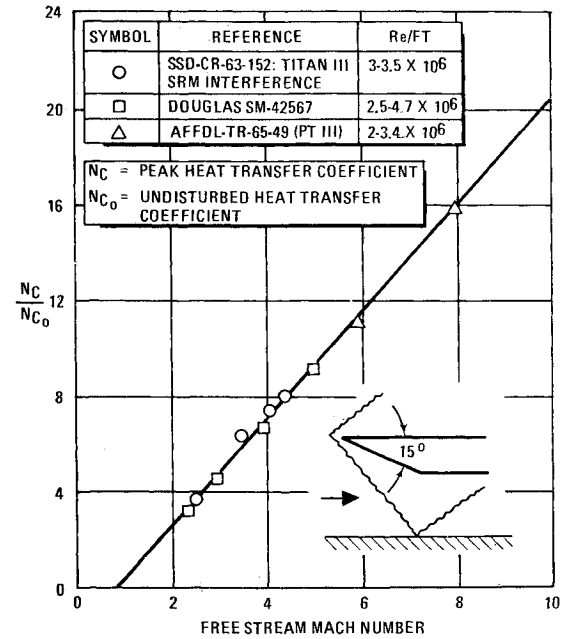

Fig. 8 Shock wave interference heating.

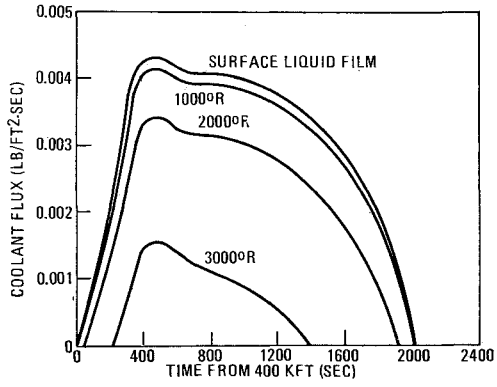

Fig. 9 Leading-edge average coolant flux.

coolant requirement in regions removed from the stagnation line.‡ The distribution for laminar flow is $\dot{m}/\dot{m}_{stag} = \cos\theta$, and for turbulent flow is $\dot{m}/\dot{m}_{stag} = \cos^{1.6}\theta$.

For the turbulent interference heating region, the transpiration cooled zone extends to an effective surface angle of 90° from the stagnation line. Outside the interference heating region the transpiration zone extends only to 80° from the stagnation line, as at that angle heating is reduced to a level compatible with the use of coated columbium.

Leading-Edge Cooling Requirements

Utilizing the previous analysis methods, average coolant fluxes were evaluated for the heating history of Fig. 7, and are presented in Figs. 9 and 10 for several assumed operating surface temperatures. Coolant fluxes are higher for the interference region, and for both cases increased surface temperature has a significant effect on reducing required coolant flux. Integrated coolant requirements are summarized in Table 1.

Buffer Layer and Structure Requirements

Thickness

In order to permit stable operation at elevated surface temperature, sufficient buffer layer must be applied to the leading edge to keep coolant phase change from occurring in the metallic structure. Required buffer layer thickness can be evaluated by selecting sizing coolant fluxes that are some fraction of the peak flux,§ and then applying them to the parametric data in Fig. 5. It can be readily seen that coolant fluxes of the low level required outside the interference region would result in excessively thick and heavy buffer layers in order to permit high-surface temperature operation. The minimum

Table 1 Leading-edge coolant summary

Surface temperature, °R	Coolant weight, lb/ft²	
	Without interference	With interference
Liquid film	6.1	196
1000	5.9	181
2000	4.4	144
3000	1.1	110
4000	...	81
5000	...	58

‡ See Fig. 1 for the relative effect of surface temperature on coolant requirement at various heating levels.

§ A weight trade could be conducted to optimize the design coolant flux for each surface temperature.

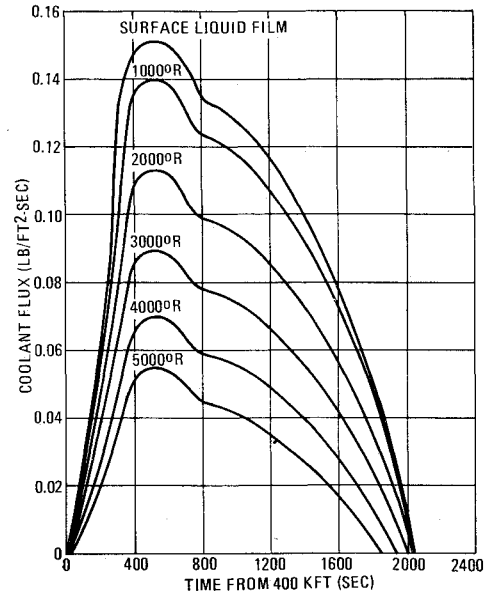

Fig. 10 Interference region average coolant flux.

weight system would consist of cooling with a liquid film directly on the surface of the porous metallic structure. For the interference region, however, coolant fluxes are sufficiently high to permit high-temperature operation with reasonable buffer layers. Table 2 presents zirconia buffer layer thickness based on 50% porosity and 25% peak coolant flux.

Porous stainless steel or perhaps a porous high-strength alloy would provide an adequate structure for the leading edge. Temperatures would be maintained low due to the transpiration cooling, and in the interference region the structure would be protected by the zirconia buffer layer. In order to be self supporting a thickness of 0.050 in. should be adequate.

Permeability

As indicated in Fig. 6, the permeability of both the metal structure and zirconia buffer layer are a function of available reservoir pressure. A supply pressure of 50 psia is adequate for coolant expulsion and does not result in high stressing of the porous structure. Table 3 presents buffer layer and structure permeability as a function of surface temperature for the interference region. The permeabilities for the structure are selected based on the peak values of coolant flux in Fig. 10 for each temperature. Outside the interference region the peak coolant flux required to maintain liquid film coverage on the structure results in a structure permeability of 1.0×10^{-13} in.².

Compacted and sintered stainless steel powder has undergone extensive development for re-entry applications, and is available in the permeability range of 1.0×10^{-14} in.² to 1.0×10^{-9} in.². Porous zirconia can be produced by a variety of methods, however in the permeability range of interest, chemical consolidation appears to be satisfactory. Figure 11 presents the results of a study of the effect of

Table 2 Interference region buffer thickness

Surface temperature, °R	Thickness, in.
1000	0.037
2000	0.078
3000	0.135
4000	0.220
5000	0.370

Table 3 Interference region permeability requirements

Surface temperature, °R	Structure permeability, in.^{2}	Buffer permeability, in.^{2}
1000	3.2×10^{-12}	3.5×10^{-10}
2000	2.6×10^{-12}	3.3×10^{-9}
3000	2.1×10^{-12}	1.0×10^{-8}
4000	1.6×10^{-12}	2.0×10^{-8}
5000	1.2×10^{-12}	3.0×10^{-8}

consolidation parameters on zirconia permeability. Phenolic microballoons were included in the mixture, and when cooked out during the curing process, yielded good permeability control.

Comparison with Other Thermal Protection Concepts

In addition to transpiration cooling, two other leading-edge concepts were analyzed. These are inhibited carbon-carbon and an ablative.¶ All three configurations are illustrated in Fig. 12. For simplicity a cylindrical contour has been assumed with a radius of 0.148 ft.

The transpiration leading edge includes a porous metallic structure fairing into the adjacent heat shield. In order to provide a coolant supply passage, a ribbed cylindrical backup, 0.03 in. in thickness, is utilized. A coolant reservoir weight of 10% the coolant weight is assumed. Pressure for coolant expulsion is assumed to be supplied by the helium pneumatic control system onboard the vehicle.

The carbon-carbon leading edge consists of a 0.2 in. thick inhibited carbon-carbon outer shell with three inner layers of insulation between the shell and the substrate. As suggested in Ref. 6 the three insulators are 0.54 in. thick zirconia foam, 0.75 in. thick Dynaflex, and 0.1 in. thick Microquartz. A titanium substructure 0.08 in. thick was assumed and included in the weight analysis. Maximum substructure temperature was limited to 600°F. The carbon-carbon shell covered 160° of the cylindrical portion of the leading edge outside of the interference region. Inside the interference region, a carbon-carbon block, 2.5 in. thick, is required to protect against burn through caused by the increased heat transfer.

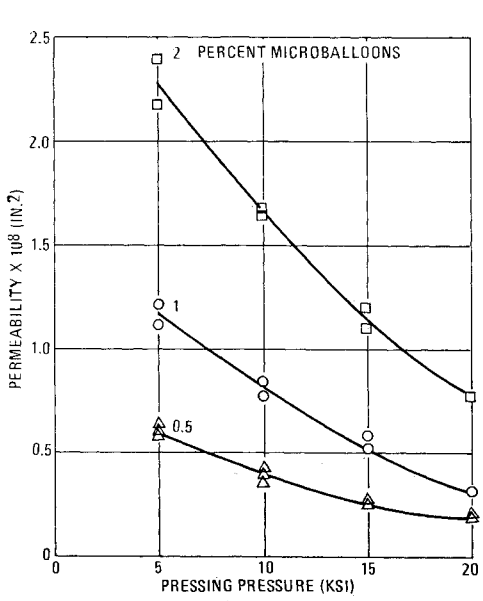

Fig. 11 Permeability of chemically consolidated zirconia.

¶ Martin SLA-561.

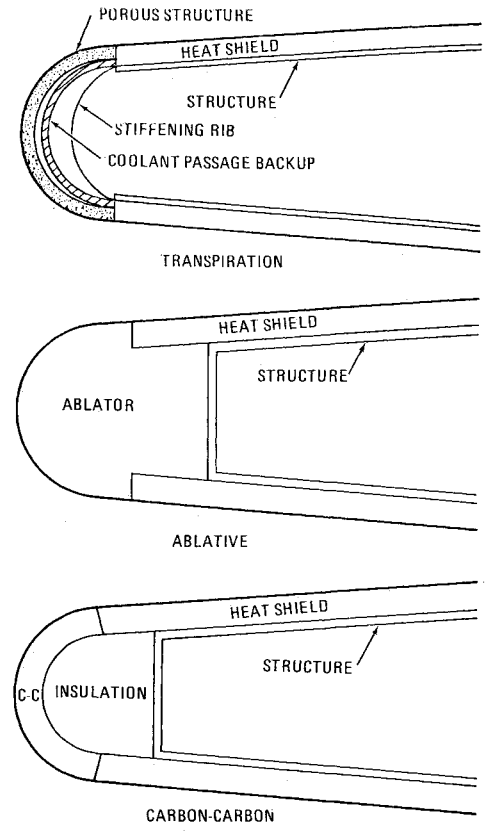

Fig. 12 Leading-edge concepts.

The ablative leading edge was constructed of a solid block of material, 2.5 in. thick. Insulation was not included in this design. This results in a simple low-weight system. The ablative surface extends just aft of the cylindrical portion. A 0.08 in. thick titanium substructure is included in the total system weight. Because of the extremely large recession which would be experienced by an ablative within the interference region, this system was not considered for use in these areas.

Weight comparisons and the results of surface recession calculations are shown in Table 4. As can be seen the ablative material results in the least weight and the transpiration design is the heaviest. The total weight, assuming a 90-ft leading edge is quite small when compared to the total vehicle thermal protection requirement. This indicates that other factors should also be considered in the selection of a leading-edge thermal protection system.

Table 5 lists a number of important parameters which must be considered. With the exception of initial cost, complexity, and flight experience the transpiration system is the preferred approach. Transpiration cooled leading edges are capable of significant reuse since they are designed to allow no degradation. Since they will not degrade and are not heating

Table 4 Leading-edge weight comparison

Thermal protection system	Unit weight, lb/ft^2	Total weight, lb	Recession, in./flight
Liquid film transpiration (including coolant and reservoir)			
Aluminum structure	7.7	322	0
Stainless steel structure	9.5	398	0
Inhibited carbon-carbon	4.93	206	0.002
Ablative	2.92	122	0.25

Table 5 Comparison of leading-edge thermal protection systems

Consideration	Ablative	Carbon-carbon	Transpiration
Reuse potential	none	low	high
Development risk	low	high	low
Configuration flexibility	minimal	low	high
Mission flexibility	low	medium	high
Packaging	difficult	difficult	simple
Flight experience	high	low	low
Initial cost	low	unknown	high
Impact damage resistance	low	low	high
Complexity	low	medium	high
Interference region use	no	marginal	yes
Inspection	difficult	difficult	simple
Thermal shock resistance	high	low	high

rate limited, they provide a much greater potential for changes in mission and configuration. No insulation is required which reduces the packaging problem. In addition, a transpiration system is the most resistant to erosion caused by rain, ice, or dust impingement.

Conclusions

The following conclusions are given based on the analysis, weight estimates, and discussion that has been presented. 1) Transpiration cooling with high-surface temperature can result in significant reductions in cooling requirement. 2) Due to the pressure drop characteristics of gases, an operational instability can occur at high-surface temperature, resulting in possible structural failure. 3) A dual layer structure, consisting of porous zirconia applied to a porous sintered metallic substrate shows promise of permitting stable high-surface temperature operation. 4) The permeability requirements for these materials can be easily met by existing fabrication methods. 5) For space shuttle type vehicles, normal leading-edge heating is not high enough to result in a weight saving for the high-temperature concept. This is because excessively thick zirconia layers are required. For interference heating however, only thin zirconia layers are required and significant over-all weight savings can be achieved. 6) Liquid film transpiration cooling can provide shape stable reuseable thermal protection for the leading edge of space shuttle type vehicles, and does not result in an excessive weight penalty.

References

[1] Click, P. L. and Schmitt, D. A., "Thermal Mapping Investigation MDC/MMC Phase B Space Shuttle Vehicles," Langley Research Center Wind Tunnel Test Results Data Rept. DMS-DR-1036, Nov. 1970, NASA.

[2] Gorowitz, H. S. and Raparelli, R. S., "Investigation of Configuration Effects on Heat Transfer Distributions and Definition of Interference Heating Areas on Space Shuttle Orbiter Configurations," Langley Research Center Wind Tunnel Test Results Data Rept. DMS-DR-1056, Jan. 1971, NASA.

[3] Gaumer, G., "Space Shuttle Data, Thermal Environment/Gas Dynamics Heating," MDC E0400, June 1971, McDonnell Douglas Corp., St. Louis, Mo.

[4] Cleary, J. W., "Lee Side Flow Phenomena on Space Shuttle Configurations at Hypersonic Speeds, Part I Flow Separation and Field Viscous Phenomena of a Delta Wing Orbiter Configuration," *Proceedings of Space Shuttle Aerothermodynamics Technology Conference*, NASA Ames Research Center, Moffett Field, Calif., Dec. 1971.

[5] Qutler, T., Rakich, J. V., and Mateer, G. G., "Application of Shock Capturing and Semi-Characteristic Methods to Shuttle Flow Fields," *Proceedings of Space Shuttle Aerothermodynamics Technology Conference*, NASA Ames Research Center, Moffett Field, Calif., Dec. 1971.

[6] Parks, D. L. and Bauer, P. E., "Leading Edge Trade Study of Thermal Protection System Unit Weight and Cost for Delta and Straight Wing Orbiters," O-EAST-TPS-6, March 1971, McDonnell Douglas Corp., St. Louis, Mo.

[7] Gomez, A. V., Curry, D. M., and Johnston, C. J., "Radiative, Ablative, and Active Cooling Thermal Protection Studies for the Leading Edge of a Fixed-Straight Wing Space Shuttle," *Proceedings of AIAA 6th Thermophysics Conference*, AIAA, New York, April 1971.

[8] Bartle, E. R. and Leadon, B. M., "The Effectiveness as a Universal Measure of Mass Transfer Cooling for a Turbulent Boundary Layer," *Proceedings of the 1962 Heat Transfer and Fluid Mechanics Institute*, Univ. of Washington, Seattle, Wash., June 1962.

[9] Rubesin, M. W., "An Analytical Estimation of the Effect of Transpiration Cooling on the Heat-Transfer and Skin-Friction Characteristics of a Compressible Turbulent Boundary Layer," TN 3341, Dec. 1954, NASA.

[10] Arne, C. L., "Ablative Materials Subject to Combustion and Thermal Radiation Phenomena," Douglas Paper 1851, Jan. 1964, McDonnell Douglas Corp., Santa Monica, Calif.